Available online at www.sciencedirect.com
SCIENCE DIRECT®
Journal of Catalysis 222 (2004) 499–510
JOURNAL OF CATALYSIS
www.elsevier.com/locate/jcat

Oxidation of CO on a Pt/Al_2O_3 catalyst: from the surface elementary steps to light-off tests
V. Experimental and kinetic model for light-off tests in excess of O_2

Abdennour Bourane and Daniel Bianchi *

Laboratoire d'Application de la Chimie à l'Environnement (LACE), UMR 5634, Université Claude Bernard, Lyon-I, Bat. 303, 43 Bd du 11 Novembre 1918, 69622 Villeurbanne, France

Received 28 July 2003; revised 30 October 2003; accepted 3 November 2003

Abstract

This article is the final part of a study on the CO/O_2 reaction over a 2.9% Pt/Al_2O_3 in line with the microkinetic approach of the heterogeneous gas–solid catalysis. Mainly, the kinetic parameters of each elementary step of two kinetic models (Models M1 and M2) determined previously are used to explain the evolution of the coverage of the adsorbed CO intermediate species (a strongly adsorbed linear CO species on Pt^0, denoted by L) as well as the turnover frequency (TOF in s^{-1}) during light-off tests (increase in the reaction temperature T_r) using 1% $CO/x\%$ O_2/He gas mixtures with $x \leqslant 50$. Model M1 involves a L-H elementary step between L CO species and a weakly adsorbed oxygen species (O_{wads}). It is operative (a) whatever T_r in excess CO and (b) only at low T_r values in excess O_2. Model M2 involves a L-H elementary step between a L CO and a strongly adsorbed oxygen species: O_{sads} is operative at high T_r values in excess O_2. It is shown that the switch for M1 to M2, at the ignition process, during the heating stage occurs for a high CO conversion (> 60%) at a specific T_r value (denoted by T_i) depending on the oxygen partial pressure. Similar to the observations on Pt single crystals, it is shown that the ignition process is associated with a surface-phase transformation from a Pt surface mainly covered by L CO species (denoted by Pt–CO) to a Pt surface mainly covered by O_{sads} (denoted by Pt–O). The Pt–CO → Pt–O transformation is due to an oxidative removal of the adsorbed L CO species into CO_2 and not to a competitive chemisorption. The high CO conversion associated with the Pt–CO → Pt–O transformation indicates that mass-transfer processes contribute to the ignition process. During a cooling stage from $T_r > T_i$, the switch from M2 to M1 (extinction process) is associated with the surface-phase transformation Pt–O → Pt–CO at a reaction temperature $T_e < T_i$.

Keywords: CO oxidation; Pt/Al_2O_3; Kinetic modeling; Elementary steps; Surface transformation; Microkinetic

1. Introduction

In previous studies [1–4] a microkinetic approach [5] of the CO/O_2 reaction over a 2.9% Pt/Al_2O_3 catalyst has been developed in order to explain the evolution of the coverages of the adsorbed species as well as the turnover frequency (TOF) during lighting-off tests (increase in the reaction temperature T_r) using 1% $CO/x\%$ O_2/He gas mixtures. The main lines of this approach are as follows:

(a) A plausible kinetic model is proposed such as Model PM:

Step S1 Adsorption of CO,

$$CO_{(gas)} \Longleftrightarrow CO_{ads};$$

Step S2 Dissociative chemisorption of oxygen,

$$O_{2(gas)} \Longleftrightarrow 2O_{ads};$$

Step S3 Langmuir–Hinshelwood elementary step,

$$CO_{ads} + O_{ads} \rightarrow CO_{2ads};$$

Step S4 Desorption of CO_2,

$$CO_{2ads} \rightarrow CO_{2(gas)}.$$

(b) Each surface elementary step is individually characterized (nature of the adsorbed species and kinetic parameters).

* Corresponding author.
E-mail address: daniel.bianchi@univ-lyon1.fr (D. Bianchi).

0021-9517/$ – see front matter
doi:10.1016/j.jcat.2003.11.019

(c) These data are used to determine a priori the evolutions of the TOF and of the coverages with T_r.

By using FTIR spectroscopy, it has been shown that whatever the CO/O_2 ratio the main adsorbed CO species on the reduced Pt surface during the reaction at $T < 373$ K is the linear CO species on Pt^0 sites (denoted by L) characterized by an IR band at ≈ 2075 cm^{-1} [1–4]. This species is oxidized at 300 K with O_2/He mixtures [1,2]: in Model PM, CO_{ads} is identified as the L CO species. Step S1 corresponds to an adsorption equilibrium and the heats of adsorption of the L CO species at several coverages θ_L (denoted by EL_{θ_L}) have been determined by using a new experimental procedure (denoted by AEIR [6]: adsorption equilibrium infrared spectroscopy). It has been shown that (a) EL_{θ_L} linearly decreases with the increase θ_L from $EL_0 = 206$ to $EL_1 = 115$ kJ/mol [6–9] and (b) it is not affected by the presence of O_2 [4,10]. Steps S2 and S3 have been characterized studying the kinetics of the oxidation of the L CO species at $T < 350$ K with x% O_2/He mixtures [1,2]. It has been shown that step S3 involves a weakly adsorbed oxygen species (O_{ads} is substituted by O_{wads} in PM) formed without competition with the L CO species [1,2]. The rate constant of step S3 is $k_3 = A_3 \exp(-E_3/RT)$ with $A_3 \approx 10^{13}$ s^{-1} and $E_3 \approx 83$ kJ/mol [1–3]. Model PM with the substitution of O_{ads} by O_{wads} and CO_{ads} by L CO is denoted by Model M1. It has been shown that Model M1 associated with the kinetic parameters of the elementary steps allows us to determine a priori θ_L as well as the TOF (at low CO conversions < 15%) during lighting-off tests in excess CO [3].

When C and O mass balances are performed during the oxidation at 300 K of the L CO species [2] in transient regimes, it is observed that a strongly adsorbed oxygen species (denoted by O_{sads}) is formed in the course of the removal of the L CO species by oxidation. This O_{sads} species may oxidize the L CO species according to a L-H elementary step S3a: L CO + O_{sads} → CO_{2ads} (rate constant $k_{3a} = A_{3a} \exp(-E_{3a}/RT)$, but with a lower rate than that of step S3 during the L CO titration leading to a situation where L CO and O_{sads} species can be present on the surface without reaction at $T < 323$ K [1,2]. Moreover, O_{sads} can be formed in a large amount by adsorption of O_2 on the freshly reduced Pt/Al_2O_3 catalyst with a high heat of adsorption: ≈ 175 kJ/mol at $\theta_{Osads} = 1$ [2]. At $T < 673$ K, O_{sads} only can be removed from the Pt surface by reduction with CO as studied in [4]. Step S3a is involved in this reaction because L CO can be adsorbed without competition on a Pt surface covered by O_{sads} [4]. However, E_{3a} strongly depends on θ_{Osads}: 65 and 110 kJ/mol at $\theta_{Osads} = 1$ and 0.4, respectively [4]. This explains that L CO and O_{sads} can be present on the surface without any reaction at $T < 323$ K for low θ_{Osads} values while they react even at 223 K at high θ_{Osads} values [4]. This leads to the conclusion that a second kinetic Model M2 derived from Model PM can be operative during the CO/O_2 reaction considering L CO and O_{sads} as adsorbed intermediates.

In the present study we show when and how models M1 and M2 must be involved to interpret the observations (coverages and TOF) during lighting-off tests in excess of O_2 using 1% CO/x% O_2/He gas mixture for $x < 50$.

2. Experimental

Preparation and characterization of the 2.9% Pt/Al_2O_3 (in wt%, γ-Al_2O_3) catalyst have been described in previous studies [1–4,6–10]. For the FTIR study, the catalyst was compressed to form a disk ($\Phi = 1.8$ cm, weight $\approx$ 40–90 mg) which was placed in the sample holder of a small internal volume stainless-steel IR cell (transmission mode) described elsewhere [7]. This IR cell enabled in situ treatments (293–900 K) of the solid, at atmospheric pressure, with a gas flow rate in the range of 150–2000 cm^3/min. The same disk of catalyst was used for several experiments and before the CO/O_2 reaction, it was treated in situ (150 cm^3/min) at 713 K according to the following procedure: oxygen (30 min) → helium (30 min) → hydrogen (1 h) → helium (10 min). Then the solid is cooled down to T_r. The Pt dispersion of the stabilized solid is 0.6–0.5 [1–4,6–11].

The data during a light-off test were obtained as in [3]: after the pretreatment of the solid, a 1% CO/x% O_2/He mixture (total pressure = 1 atm, x in the range 0.125–50, flow rate = 200 cm^3/min) was introduced in the IR cell at 300 K and T_r was slowly increased ($\approx$ 10 K/min) up to 740 K while the FTIR spectra of the adsorbed species were recorded periodically. Then the solid was cooled down in CO/O_2 and the FTIR spectra were compared to those recorded at similar temperatures in the course of the heating stage. In order to correlate the θ_L evolutions to the CO conversion (denoted by $CO_{\%}$, i.e., $CO_{\%} = 100 \times ([CO]_{in} - [CO]_{out})/[CO]_{in}$ with [ ] the CO concentrations at the inlet and outlet of the reactor), the CO and CO_2 molar fractions at the outlet of the IR cell were determined by using a second FTIR spectrometer with an IR gas cell ($L = 20$ cm, volume 200 cm^3). Other authors have performed similar experiments on supported Pt catalysts [11–18] (see also the part dedicated to the CO/O_2 reaction in the review of Schüth et al. [19] on the oscillation regimes). However, we extended significantly the experimental conditions (i.e., higher T_r values) and we improved the exploitation of the experimental data.

In parallel to the FTIR study, lighting-off tests were performed in a quartz microreactor (powder of catalyst) [3] using experimental conditions similar to those of Cai et al. [20] (weight of catalyst $\approx$ 200 mg, flow rate in the range 100–600 cm^3/min). The composition (in molar fraction) of the gas mixtures at the outlet of the reactor was determined with a mass spectrometer (analysis frequency 1/1.5 Hz) according to a procedure previously described [2,3,11] while T_r was recorded using a small K thermocouple ($\Phi = 0.25$ mm) inserted in the catalyst powder.

3. Results and discussion

3.1. Coverage of the linear CO species for CO/O_2 ratios > 2

This has been studied in detail in [3] and we summarize below the main results to facilitate the comparison to those with an excess of O_2. For instance, Fig. 1 gives the evolution of the IR band of the L CO species (denoted by B_L) for 1% CO/0.125% O_2/He with the increase in T_r. The observations are very similar to those during the CO adsorption with 1% CO/He [3,6,8]. The increase in the intensity of B_L for $T < 400$ K has been ascribed to a reconstruction of the Pt surface while the shift and the decrease in B_L for $T_a > 540$ K is mainly due to the decrease in θ_L according to the adsorption equilibrium [3,6,8]. Moreover, cooling of the sample in 1% CO/0.125% O_2/He leads to FTIR spectra similar to those observed at the same T_r value during the heating stage, except for $T < 500$ K where B_L remains constant (irreversible reconstruction during the heating stage). Similar observations have been made with $x = 0.25$ [3]. The curves $\theta_L = f(T_r)$ have been determined using the change in the IR band area of B_L (denoted by A_L) with T_r similarly to the adsorption procedure ($\theta_L = A_L(T_r)/A_{L(max)}$). The results (curve a, Fig. 2A) clearly show that θ_L is only slightly modified by the CO/O_2 reaction as compared to the CO adsorption [3,6–8] while in parallel CO_2 is that expected for the total consumption of O_2 [3].

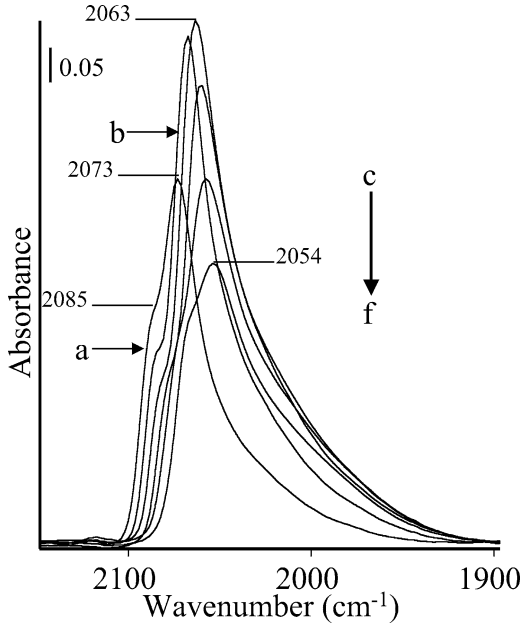

Fig. 1. FTIR spectra recorded at various temperatures in the course of a light-off test with the 1% CO/0.125% O_2/He mixture on Pt/Al_2O_3: (a–f) 351, 388, 503, 603, 663, 723 K.

3.2. Coverage of the linear CO species for $CO/O_2 = 2$

Fig. 3 gives the FTIR spectra recorded during the increase in T_r with a 1% CO/0.5% O_2/He mixture. At 320 K, B_L is detected at 2073 cm^{-1} together with a shoulder at 2085 cm^{-1}. For $T_r < 560$ K (Figs. 3a–c), there is a strong similitude in the evolutions of the FTIR spectra with those in Fig. 1: B_L shifts to lower wavenumbers (2073 and 2065 cm^{-1} at 326 and 538 K, respectively) while its intensity increases (reconstruction). The shoulder at 2085 cm^{-1} shifts to lower wavenumbers and it is no more detected at $T_r = 538$ K. For $T_r > 538$ K (Figs. 3d–j) there is a clear difference with the results observed with lower x values: B_L strongly decreases and disappears at 623 K associated with a shift to lower wavenumbers (2062, 2057, and 2054 cm^{-1} at 560, 585, and 603 K). Between 603 and 623 K, B_L is detected at the same position. It must be noted that B_L strongly decreases in a short T_r range: 585–623 K. However, there are no difficulties in following experimentally this progres-

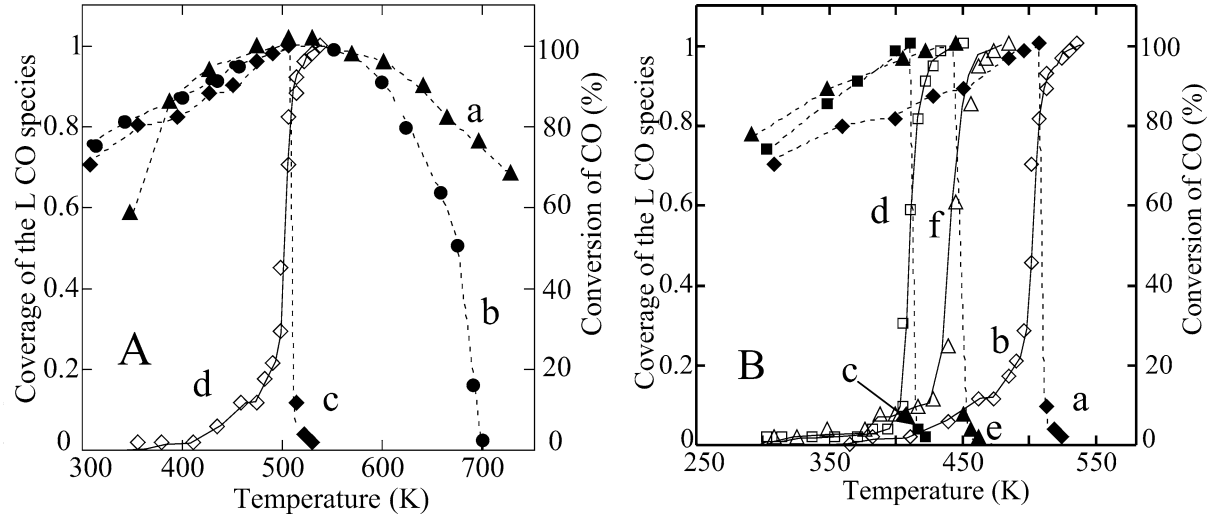

Fig. 2. (A and B) Evolution of the coverage of the L CO species θ_L (solid symbols) and CO_2 conversion (open symbols) for various 1% CO/x% O_2/He mixtures on 2.9% Pt/Al_2O_3: (A) (a) $x = 0.125$ (CO% not shown); (b) $x = 0.5$ (CO% not shown); (c and d) $x = 1$. (B) (a and b) $x = 1$; (c and d) $x = 50$; (e and f) $x = 10$.

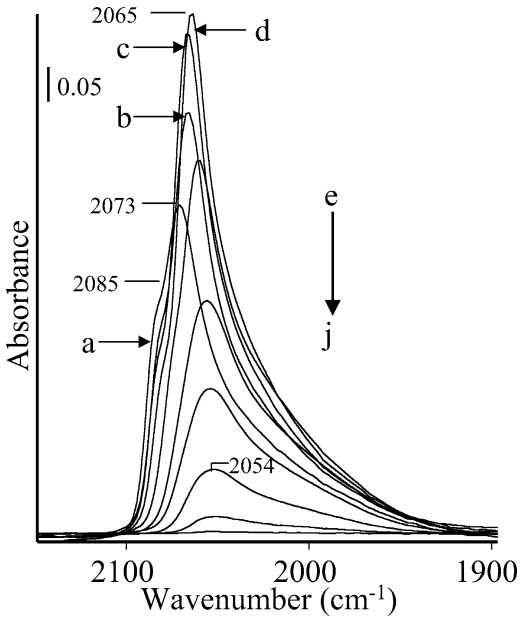

Fig. 3. FTIR spectra recorded at various temperatures in the course of a light-off test with 1% CO/0.5% O_2/He mixture: (a–j) 326, 438, 470, 538, 585, 603, 608, 613, 618, 623 in K.

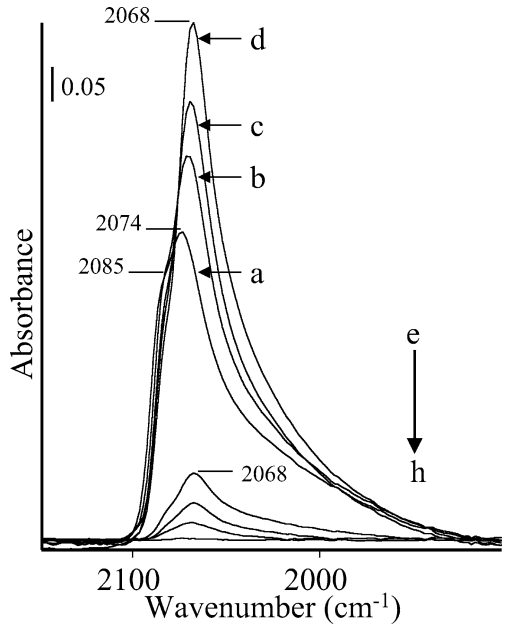

Fig. 4. FTIR spectra recorded at various temperatures in the course of a light-off test with 1% CO/1% O_2/He mixture: (a–h) 306, 398, 452, 507, 511, 513, 523, 543 in K.

sive decrease. The evolution of θ_L with T_r is shown in curve b in Fig. 2A. By comparison with curve a in Fig. 2B it can be observed that the oxidation reaction strongly modifies the adsorption equilibrium at $T > 600$ K for $x = 0.5$.

3.3. Coverage of the linear CO species for $CO/O_2 < 2$

Fig. 4 gives the evolution of the IR spectra with T_r using 1% CO/1% O_2/He. For $T_r < 507$ K (Figs. 4a–d), the observations are similar to those in Figs. 1 and 3. B_L is detected at 2074 cm^{-1} at 300 K, and then it increases (reconstruction) and shifts to lower wavenumbers (2068 cm^{-1} at 507 K). The shoulder at 2085 cm^{-1} contributes significantly to the spectrum at 306 K but it shifts to lower wavenumbers with the increase in T_r and it is no more detected at 507 K. The evolution of the spectra at $T_r > 507$ K is strongly different than in Figs. 1 and 3. In a short T_r range, 507–511 K, there is an abrupt decrease in B_L. However, B_L is still detected at 2068 cm^{-1} for $T_r = 511$ K (spectrum e). Then it decreases progressively without any shift and finally disappears at 543 K. The abrupt decrease in B_L at a given T_r value has also been observed by other authors on Pt catalysts [12,17] and this process is called ignition [12]. The T_r value where the jump is detected is called ignition temperature T_i [12] (i.e., with $x = 1$, $T_i = 507$ K). Curve c in Fig. 2A gives the evolution of θ_L with T_r for $x = 1$. Similar results have been observed for $x > 1$; however, the higher P_{O_2}, the lower T_i. For instance, Fig. 5 gives the evolution of the FTIR spectra recorded with the 1% CO/50% O_2/He mixture: B_L is detected at 2079 cm^{-1} at low temperatures (Fig. 5a). For $T_r < 410$ K, the results are similar to those observed in Figs. 1, 3, and 4: B_L shifts to lower wavenumbers and its intensity increases (Fig. 5a–e). At $T_i = 413$ K,

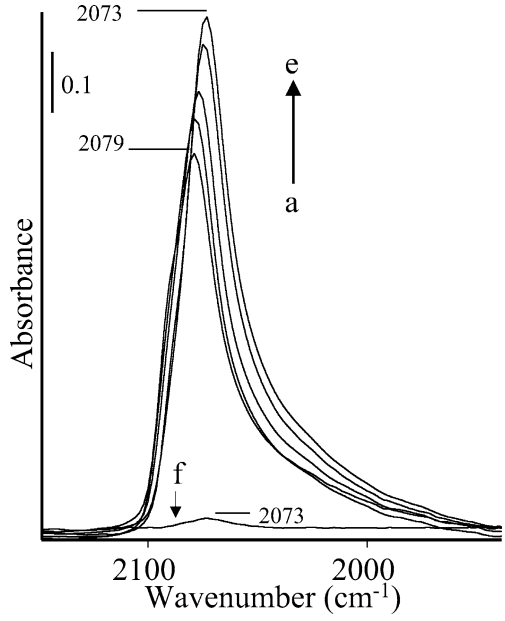

Fig. 5. FTIR spectra recorded at various temperatures in the course of a light-off test with 1% CO/50% O_2/He mixture: (a–f) 304, 318, 348, 393, 410, 415 in K.

B_L abruptly decreases but it is still detected at 2073 cm^{-1} at $T_r = 425$ K and then it progressively decreases (exponential profile) and disappears at 450 K. Curve c in Fig. 2B gives the evolution of θ_L for 1% CO/50% O_2/He. The profile is similar to that observed with $x = 1$ (curve a, Fig. 2B) but clearly T_i is lower. We have performed similar experiments with $x = 2$ and 10 and curve e in Fig. 2B gives $\theta_L = f(T_r)$ for $x = 10$. Note that T_i progressively decreases with the increase in P_{O_2}: 507, 463, 443, and 413 K for $x = 1$, 2, 10,

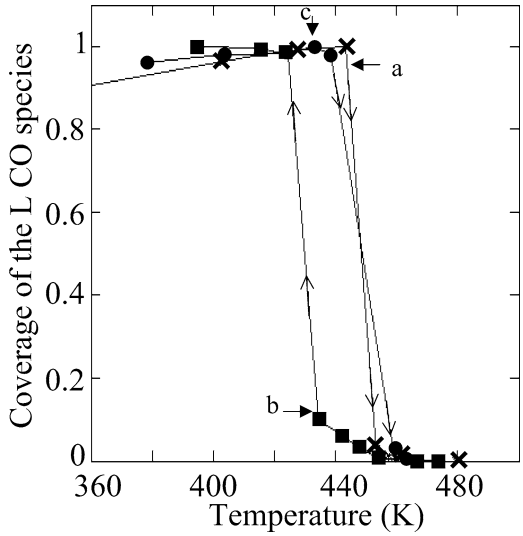

Fig. 6. Evolutions of θ_L with 1% CO/10% O_2/He in the course of heating and cooling stages (×, a) first heating stage; (■, b) cooling stage; (●, c) second heating stage.

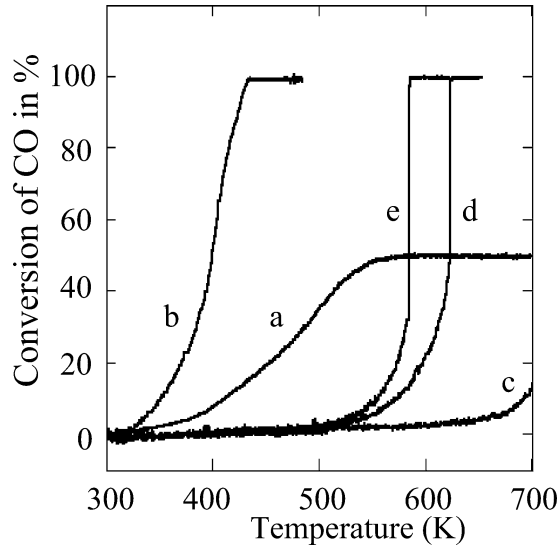

Fig. 7. CO conversion during light-off tests in the quartz microreactor according to various experimental conditions using 1% CO/x% O_2/He: (a) $w_{Pt/Al_2O_3} = 0.41$g, $x = 0.25$, $F = 600$ cm^3/min; (b) $w_{Pt/Al_2O_3} = 0.41$g, $x = 3$, $F = 600$ cm^3/min; (c) empty reactor, $x = 5$, $F = 100$ cm^3/min; (d) $w_{Al_2O_3} = 0.32$g, $x = 5$, $F = 100$ cm^3/min; and (e) $w_{Al_2O_3} = 0.32$g, $x = 50$, $F = 100$ cm^3/min.

and 50, respectively. For CO/O_2 ratios < 2, it is impossible even by increasing T_r very slowly, to follow the decrease in B_L at T_i (at the opposite of Fig. 3): a small increment in T_r is enough to create the abrupt decrease in B_L. The analysis of the gas mixture at the outlet of the IR cell reactor allows us to follow the evolution of $CO_{\%}$ in parallel with θ_L (curves b, d, and f for $x = 1$, 50, and 10 in Fig. 2B). These curves show that the abrupt decrease in θ_L at T_i occurs at $CO_{\%} > 60\%$. This is in good agreement with the observations of Kaul and Wolf [12] during the increase in T_r with a 3.8% CO/2.1% O_2/N_2 mixture on 5% Pt/SiO_2: $T_i = 538$ K for $CO_{\%} \approx 40\%$ (Fig. 3 in [12]).

Fig. 6 gives the evolution of θ_L with 1% CO/10% O_2/He during the increase (Fig. 6a) and the decrease (Fig. 6b) in T_r. It can be observed that there is a hysteresis: θ_L abruptly decreases at T_i in Fig. 6a during the heating stage while it increases abruptly during the cooling stage (extinction process [12,17]) at $T_e < T_i$. During the cooling stage for $T_r > T_e$, θ_L increases progressively (exponential profile) to values higher than those observed after T_i. Fig. 6c which overlaps with curve a is obtained after a new increase in T_r after curve b, indicating the reproducibility of the experiments. Similar hystereses are observed for CO/O_2 ratios < 2 but not for $CO/O_2 > 2$. The results described in the present study are mainly obtained during the increase in T_r and we have not observed the development of an oscillation regime in agreement with Kaul and Wolf who observe oscillations on catalyst disks only during slow cooling stages [23].

3.4. Evolution of the CO conversion during lighting-off tests on Pt/Al_2O_3 and Al_2O_3

As shown in Part III [3] the correlation between theoretical (TOF_{th}) and experimental (TOF_{ex}) TOF values during lighting-off tests only can be performed for $CO_{\%} < 15\%$. For these values the accuracy using the CO and CO_2 signals at the outlet of the IR cell reactor is limited due to the mixing in the IR gas cell. The CO conversions have been determined with the quartz microreactor similarly to Cai et al. [20] ($m = 0.4$ mg, flow rate 600 cm^3/min, 1% CO/x% O_2/He gas mixtures). Figs. 7a and b show $CO_{\%} = f(T_r)$ (using the CO molar fraction) on 2.9% Pt/Al_2O_3 with $x = 0.25$ and $x = 3$, respectively. For $x = 0.25$, the maximum conversion is that excepted for the total O_2 consumption while CO is totally converted for $x = 3$. Moreover, for $x = 3$ there is no abrupt increase in $CO_{\%}$ in parallel to the abrupt decrease in θ_L at T_i (Fig. 2) in agreement with the observations on Pt/SiO_2 [12,13] and Pt/Al_2O_3 [18]. Note that the curves $CO_{\%} = f(T_r)$ in Figs. 2 and 7 cannot be compared without considering the differences in the experimental conditions (weight of catalyst and gas flow rate). For O_2/CO ratios > 5, Cai et al. [20] indicate that blank experiments performed with the Al_2O_3 support alone may lead to light-off curves similar to those observed on noble metal-supported catalysts but shifted to higher temperatures. However, for $O_2/CO = 50$ the conversion curves for Al_2O_3 and Pt/Al_2O_3 are overlapped (see Figs. 2 and 3 in [20]). This contribution of the blank to $CO_{\%}$ must be evaluated in order to interpret correctly the correlations between $\theta_L = f(T_r)$ and $TOF = f(T_r)$. We have verified that the homogeneous reaction does not significantly contribute to $CO_{\%}$ by using an empty reactor with a 100 cm^3/min flow rate of 1% CO/5% O_2/He (curve c in Fig. 7). For $x < 0.5$, blank experiments performed with the Al_2O_3 support (0.34 g, flow rate 100 cm^3/min) indicate that $CO_{\%}$ is negligible [4] (i.e., for $x = 0.25$, $CO_{\%} = 1.5\%$ at 740 K). For $x > 1$, the contribution of the support is more significant as shown in

Figs. 7d and e for $x = 5$ and 50, respectively. However, it can be observed that the support converts CO at higher T_r values than Pt/Al_2O_3. This indicates that, under our experimental conditions, the Al_2O_3 support does not contribute significantly to the CO_2 production in the presence of Pt even with an O_2/CO ratio of 50, opposite to the observations of Cai et al. [20]. However, the authors [20] use a different Al_2O_3 support with a higher BET area (256 m^2/g compared to 110 m^2/g in the present study) and the light-off tests are performed with 1 g of support compared to 0.3 g in the present study.

3.5. *Theoretical curves for* $\theta_L = f(T_r)$ *and* $TOF = f(T_r)$ *before* T_i

Before T_i, the Pt surface is covered by the L CO species ($\theta_L = 1$) whatever $x < 50$ in 1% CO/x% O_2/He. This allows us to consider that Model M1 (reaction between L CO and O_{wads}) used to obtain the theoretical curves in excess CO [3] remains valid in excess of O_2. The mathematical procedure has been described in detail in [3] and we summarize the main steps for the comparison with Model M2. We assume that (a) there is a steady state at each T_r value between the rate of adsorption (R_a) and the two rates of desorption (R_d) and of oxidation (R_o),

$$R_a - R_d - R_o = 0 \tag{1}$$

and (b) there is no competition between L CO and O_{wads} leading to

$$k_a P_{CO}(1-\theta_L) - k_d\theta_L - k_3\theta_{Owads}\theta_L = 0, \tag{2}$$

where P_{CO} is the partial pressure of CO, k_a and k_d are the rate constants of adsorption and desorption, respectively, while θ_L and θ_{Owads} are the coverages of the L and O_{wads} species. Expression (2) leads to

$$\theta_L = \frac{K_{CO}P_{CO}}{1 + K_{CO}P_{CO} + K_{ox}\theta_{Owads}}, \tag{3}$$

where $K_{CO} = k_a/k_d$ is the adsorption coefficient for the L species given by [1–4,6–10,21,22],

$$K_{CO} = \frac{h^3}{k(2\pi mk)^{3/2}}\frac{1}{T_a^{5/2}}\exp\left(\frac{E_d - E_a}{RT_a}\right), \tag{4}$$

and $K_{ox} = k_3/k_d$ is an oxidation coefficient by analogy with K_{CO} [3]. The rate constant of desorption is given by $k_d = (kT/h)\exp(-E_d/RT)$ with E_d varying with θ_L as the heat of adsorption [4]. The coverage of O_{wads} specie is given by [3]

$$\theta_{Owads} = \sqrt{K_{O_2}P_{O_2}}, \tag{5}$$

where K_{O_2} is the adsorption coefficient of O_{wads} given by (4) with $m = 32 \times 10^{-3}$ kg/6.02×10^{23}) and $E_{O_2} \approx$ 30 kJ/mol [1,2].

The theoretical curves $\theta_L = f(T_r)$ are obtained [3] solving numerically expression (3) for given P_{CO} and P_{O_2} values and considering a linear variation of $E_{\theta L}$ with θ_L [6–10]. It has been shown that $E_{\theta L}$ varies linearly from $E_0 = 195$ to $E_1 = 122$ kJ/mol [3]. The theoretical TOF_{Th} [24] is obtained numerically [3] according to step S3,

$$TOF_{th} = R_o = k_3\theta_L\theta_{Owads}, \tag{6}$$

with θ_L and θ_{Owads} given by (3) and (5), respectively. During a lighting-off test for $T_r < T_i$, θ_L and TOF_{th} are obtained from expressions (3) and (6), respectively, considering that the various kinetic parameters are those determined studying each elementary step [1–11]. For the rate constant $k_3 = (kT/h)\exp(-E_3/RT)$ the value of E_3 is 83 kJ/mol as used in [3] for $x < 0.5$.

In excess CO, there is a good agreement [3] between experimental and theoretical curves $\theta_L = f(T_r)$ and $TOF = f(T_r)$. In particular, it has been shown that $\theta_L = f(T_r)$ is similar to $\theta_L = f(T_a)$ during adsorption because (a) step S3 does not disturb strongly the adsorption equilibrium and (b) the presence of oxygen does not change the heat of adsorption of the L CO species [10]. These conclusions are also valid in excess O_2: kinetic modeling using Model M1 indicates (see Fig. 10a for $x = 10$) that the theoretical curves $\theta_L = f(T_r)$ only differ slightly from the adsorption equilibrium curve $\theta_L = f(T_a)$ [6–10] at $T_r > 600$ K due to the impact of step S3. In particular, it must be concluded that Model M1 alone cannot explain the abrupt decrease in θ_L at T_i. For $T_r < T_i$, Figs. 8a and b give TOF_{ex} while Figs. 8c and d give TOF_{th} from Model M1 for $x = 0.25$ and 3, respectively. It can be observed that there is a good agreement between TOF_{ex} and TOF_{th} values for $CO_{\%} \lesssim 5\%$ ($CO\% = 11\%$ at $TOF_{ex} = 0.02$). Similar to [3], assuming that E_3 increases slightly (due to the coverages) in the range 83 to 91 kJ/mol for the temperature range in Fig. 8 leads (Figs. 8e–f) to an agreement on a larger TOF range. For high $CO_{\%}$ values, mass-transfer processes limit TOF_{ex} that is strongly lower than TOF_{th}. For instance, at high temperatures TOF_{th} for $x = 0.25$ is much higher (100 s^{-1}) than that needed to convert totally CO (≈ 0.2 s^{-1}). It can be observed in Fig. 2B that there is a limited difference between the experimental $CO_{\%} = f(T_r)$ curves d and f for $x = 50$ and 10. This agrees very well with the fact that the $TOF_{th} = f(T_r)$ curves obtained for $x = 3$ (Fig. 8f) and $x = 50$ (Fig. 8g) do not strongly differ. Moreover, the calculations indicate that θ_L remains ≈ 1 even for TOF_{th} as high as 300 s^{-1} in agreement with the fact that FTIR results show that B_L remains $\approx$ constant below T_i at $CO_{\%} \lesssim 60\%$.

Finally, it must be considered that Model M1 associated with the kinetic parameters determined studying individually each elementary step allows us to interpret the curves $TOF = f(T_r)$ and $\theta_L = f(T_r)$ in the absence of the ignition process for 1% CO/x% O_2/He gas mixtures with $x < 50$. A conclusion of this kinetic modeling is that the abrupt decrease in θ_L at T_i for $CO_{\%} > 60\%$ is not explained only by Model M1 and a second factor must be involved.

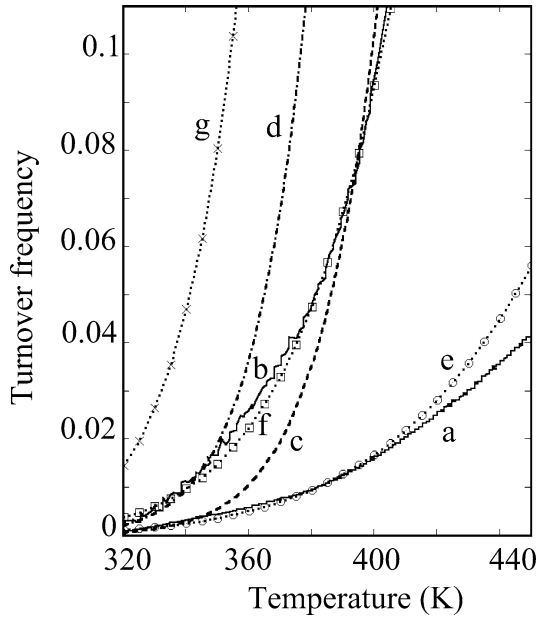

Fig. 8. Comparison between the experimental TOF_{ex} and theoretical TOF_{th} values during light-off tests according to Model M1 for 1% CO/x% O_2/He: (a and b) TOF_{ex} for $x = 0.25$ and $x = 3$, respectively; (c and d) TOF_{th} for $x = 0.25$ and $x = 3$, respectively; (e, f, and g) TOF_{th} for $x = 0.25$, $x = 3$, and $x = 50$, respectively, considering that E_3 slightly increases with the decrease in coverages (see the text for more details).

3.6. Composition of the Pt surface after T_i

The FTIR spectra (Figs. 3–5) clearly show that L CO species dominates the coverage of the Pt surface in excess O_2 for $T_r < T_i$ while at T_i there is an abrupt decrease in θ_L from ≈ 1 to $\lesssim 0.15$ followed by a progressive decrease to 0 for $T_r > T_i$ (Figs. 4 and 5). It has been shown previously that the oxidative removal of L CO at 300 K with x% O_2/He mixtures leads to the increase in θ_{Osads} [2]. This suggests that a similar increase in θ_{Osads} is associated with the ignition process as confirmed by the experiments in Fig. 9. A 1% CO/2% O_2/3% Ar/He mixture is introduced at $T_r = 630$ K $> T_i$ leading to $CO_{\%} \approx 100\%$ (Fig. 9A). Then after a short purge in helium (Fig. 9B) to remove the gas phase, a 1% CO/2% Ar/He mixture is introduced for the titration of the O_{sads} species as performed in [4]. It can be observed in Fig. 9C by comparing the Ar and CO curves that a large amount of CO is consumed: 172 μmol/g, due to two main processes (a) the oxidation of O_{sads} species and (b) the CO adsorption to form the L CO species at a coverage ≈ 0.93 in the absence of O_2 [1–3,6–10]. The CO_2 production during the titration in part C is 110 μmol/g leading to an amount of adsorbed CO species of 62 μmol/g, in reasonable agreement with the coverage expected at 630 K [2,6–10]. Moreover, the plateau profile of the CO_2 peak in part C is characteristic of the O_{sads} titration for $T > 350$ K due to the control of the CO_2 production by mass-transfer processes [4]. At 630 K, other processes may contribute to the CO_2 and CO signals during the titration such as the desorption of carbonate species from the support and the CO disproportionation

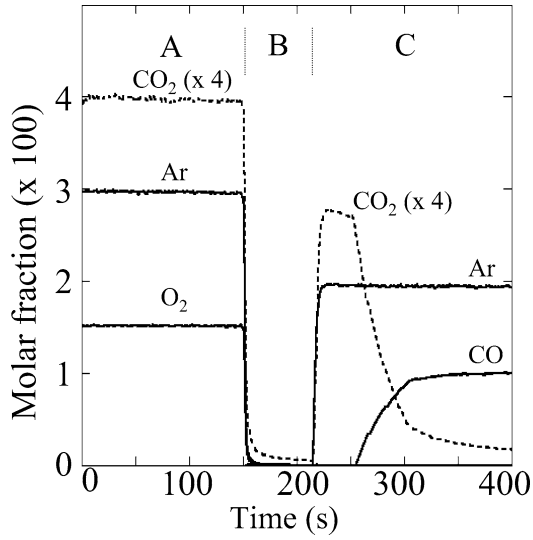

Fig. 9. Molar fractions of the gases during the titration of the O_{sads} at 640 K after the ignition: (A) CO/O_2 reaction with 1% CO/2% O_2/3% Ar/He; (B) in helium; (C) titration with 1% CO/2% Ar/He.

on the Pt particles. For instance, the alumina support may adsorb 19 μmol of CO_2/g and in Fig. 9B it can be see that CO_2 desorbs during the helium purge (8 μmol/g) and the remaining fraction (≈ 10 μmol/g) may desorb during the titration. Moreover, the final part of the CO_2 production in part C probably comes from the CO dissociation. Assuming a constant rate of dissociation during the titration indicates a contribution of ≈ 6 μmol/g of CO_2. We may roughly estimate that ≈ 94 μmol/g of CO_2 comes from the titration of the O_{sads} species. This value exceeds the amount of adsorbed O_{sads} on a freshly reduced surface (≈ 70 μmol O/g). The difference is maybe due either to the reconstruction of the catalyst or to the formation of subsurface oxygen [25] in addition to the O_{sads} species at $T_r > T_i$.

The experiments in Fig. 9 clearly show that there is a large amount of O_{sads} on the Pt surface after T_i. To facilitate the presentation, the surface states before and after T_i are denoted by Pt–CO and Pt–O, respectively. It is reasonable to consider that the CO/O_2 reaction on those two surfaces may proceed according to two kinetic models that differ according to the adsorbed intermediate species: L CO and O_{wads} on Pt–CO (Model M1) [1–3] and L CO and O_{sads} [4] on Pt–O (Model M2). This view is in line with the study of Hoffman et al. [26] which considers the involvement of two kinetic models for the CO/O_2 reaction on model Pd/Al_2O_3 catalysts to explain qualitatively transient as well as steady-state observations using molecular beams. However, on Pd/Al_2O_3 [26] the models differ by the involvement of strongly and weakly adsorbed CO species. Moreover, for the theoretical explanation of the kinetic oscillations during the CO/O_2 reaction on Pt(100) which is based on surface-phase transformations hex $\leftrightarrow 1 \times 1$, Imbihl et al. [27] consider that the reaction proceeds on the two surfaces according to the same formal series of elementary steps (similar to Model PM) but their rate constants differ

strongly according to the operative surface. This is in agreement with the M1 and M2 formalism.

3.7. Kinetic modeling of $\theta_L = f(T_r)$ after T_i

3.7.1. Theoretical curves using Model M2

The kinetic Model M2 on a Pt–O surface that derives from PM is defined as follows:

Step S1a Adsorption of CO to form a L CO species on Pt–O,

$$CO_{(gas)} \Longleftrightarrow L;$$

Step S2a Dissociative O_2 chemisorption to form O_{sads},

$$O_{2(gas)} \Longleftrightarrow 2O_{sads};$$

Step S3a L-H surface reaction,

$$L + O_{sads} \rightarrow CO_{2ads};$$

Step S4 Desorption (fast) of CO_2,

$$CO_{2ads} \rightarrow CO_{2(gas)}.$$

This model is based on the kinetic study of the reduction of O_{sads} by CO at $T < 350$ K [4]. It has been shown [4] that L CO species is adsorbed on a the Pt–O surface ($B_L = 2084\ cm^{-1}$ at 300 K) in an amount and with a heat of adsorption similar to that on a freshly reduced Pt surface (there is no competition in agreement with Pt single crystals [28,29]).

It is considered that the coverage of each adsorbed species, L CO and O_{sads}, during the CO/O_2 reaction depends on two equilibrium according to expression (1). This leads to the following equations considering the absence of competition between adsorbed species.

For the L CO species,

$$K_{CO} P_{CO}(1-\theta_L) - \theta_L - (k_{3a}/k_{dL})\theta_L\theta_0 = 0, \quad (7)$$

for the O_{sads} species,

$$K_{Osads} P_{O_2}(1-\theta_O)^2 - {\theta_O}^2 - (k_{3a}/k_{dOsads})\theta_L\theta_0 = 0, \quad (8)$$

where K_{CO}, K_{Osads}, and k_{dL}, k_{dOsads} are the adsorption coefficients and the rate constants of desorption of the L CO and O_{sads} species, respectively, k_{3a} is the rate constant of step S3a (preexponential factor: $kT/h \approx 10^{13}\ s^{-1}$). The theoretical curves for $\theta_L = f(T_r)$ and TOF $= (f(T_r)$ from Model M2 are obtained using the kinetic parameters determined previously [1–4] solving numerically Eqs. (7) and (8). The exact value of the heat of adsorption of the L CO species on Pt–O is not known. However, Figs. 4 and 5 indicate clearly that B_L is detected after T_i in favor of a high heat of adsorption in agreement with [4]. In the calculations, it is considered that it is equal to that of the L CO species formed on clean Pt particles varying linearly with the coverage from $E_0 = 195$ to $E_1 = 122$ kJ/mol as justified in [4] and in agreement with DFT calculations [30]. The heat of adsorption of the O_{sads} species formed at T_i is considered equal to that of the species formed by O_2 chemisorption on a freshly reduced Pt surface, 175 kJ/mol at $\theta_{Osads} = 1$ [2], in agreement with the measurements of Wartnaby et al. [31] on Pt(110), ≈ 155 kJ/mol at high coverages. These authors [31] have shown that the heat of adsorption of O_2 increases to 332 ± 10 kJ/mol at $\theta_{Osads} = 0$ according to a roughly linear profile. The heat of adsorption of the O_{sads} species at low coverages on Pt/Al_2O_3 has not been determined and in the present calculations we consider that its linearly varies from 175 to 330 kJ/mol at $\theta_{Osads} = 1$ [2] and 0 [31], respectively. The activation energy E_{3a} increases with the decrease in θ_{Osads} from 65 to 110 kJ/mol at $\theta_{Osads} = 1$ and 0.4 [4], respectively.

Fig. 10 compares the theoretical curves $\theta_L = f(T_r)$ and $TOF_{th} = f(T_r)$ for a 1% CO/10% O_2/He gas mixture according to Model M1 (Expressions (3) and (6), Figs. 10a and b) and Model M2 (Expressions (7) and (8), Figs. 10c and e). Fig. 10a shows that θ_L from Model M1 is slightly different from the adsorption equilibrium [6–10] for $T_r > 600$ K while Fig. 10c shows that θ_L from Model M2 differs strongly from the adsorption curve due to the impact of step S3a for $T_r > 340$ K. At $T_r > 500$ K, θ_L is very low in agreement with the fact that B_L is detected with a low intensity after T_i for 1% CO/10% O_2/He (Fig. 6). Curve d shows that θ_{Osads} obtained from Model M2 (Eq. (8)) also differs from the adsorption equilibrium ($\theta_{Osads} = 1$ for $T_a < 700$ K) due to the impact of step S3a. However, it remains high in agreement with the O_{sads} titration in Fig. 9. The TOF_{th} values according to Model M2 (Fig. 10e) are strongly higher (factor 100) than those from Model M1 (Fig. 10b). It must be noted that it is not excluded that there is a small coverage of O_{sads} species before T_i without any significant contribu-

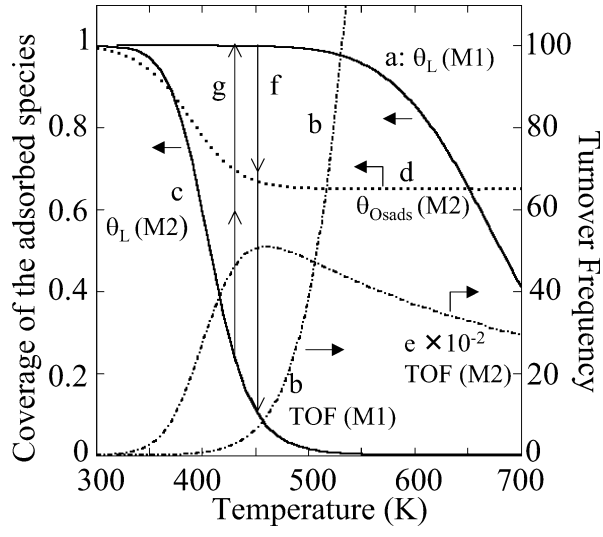

Fig. 10. Theoretical θ_L and TOF curves from kinetic Models M1 and M2 for 1% CO/10% O_2/He: (a and b) θ_L and TOF according to Model M1; (c, d, and e) θ_L, θ_{Osads}, and TOF according to Model M2 (see the text for more details); (f and g) graphical representation of the change in θ_L at T_i and T_e, respectively.

tion to the experimental TOF and θ_L curves due to the high activation energy of step S3a at low θ_{Osads} values. For instance, calculations (not shown) similar to those in Fig. 10 using Model M2 indicate that the evolutions of θ_L do not differ from the adsorption for $E_{3a} > 125$ kJ/mol.

3.7.2. Qualitative explanation of the evolution of θ_L at T_i

The experimental evolution of θ_L in excess O_2 can be interpreted as follow: for $T_r < T_i$ Model M1 is operative on the Pt–CO surface. At T_i there is a Pt–CO → Pt–O transformation and Model M2 is operative for $T_r > T_i$. This leads to an abrupt jump of θ_L from Fig. 10a (Model M1) to Fig. 10c (Model M2) as represented by curve f for a T_i value equal to that experimentally observed with 1% CO/10% O_2/He. Fig. 10c explains that θ_L is not equal to 0 after T_i in agreement with the detection and the progressive decrease of B_L in Figs. 4 and 5 for $T_r > T_i$. Note that TOF_{th} from Model M2 is strongly higher than that from Model M1 in particular after T_i (compare curves b and e in Fig. 10) and the abrupt decrease in θ_L at T_i must be associated with the abrupt increase in TOF. However, this is not observed experimentally (Fig. 2) because the ignition is associated with a high CO conversion when mass-transfer processes limit the rate of reaction [4]. A similar remark ($CO_{\%}$ does not abruptly increase at T_i) can be made with the observations of Garcia et al. [18] on Pt/Al_2O_3. Calculations with Model M2 similar to those in Fig. 10 for different P_{O_2} values (not shown) indicate that the increase in P_{O_2} shifts the curves c and e to lower T_r values explaining that θ_L after T_i depend on P_{O_2} as experimentally observed. Moreover, the increase in P_{O_2} also shifts curve b (TOF_{th} from Model M1) to lower temperatures. Assuming that the ignition process is linked to a critical value of the TOF (denoted by TOF_{ci}) the jump in θ_L from curve a to curve c (Fig. 10) must be detected at lower T_i values: this explains that the higher P_{O_2} the lower T_i (Fig. 2).

In the course of the cooling stage after an increase at $T_r > T_i$, (Pt–O surface), it is observed (Fig. 6) that θ_L increases progressively until $T_e < T_i$, where θ_L increases abruptly to 1. Curve c in Fig. 10 shows that Model M_2 offers a reasonable interpretation of the fact that $T_e < T_i$. Assuming that the switch from Model M2 to Model M1 occurs at a critical TOF_{ce} value similar to TOF_{ci} and because at a given reaction temperature TOF_{th} from Model M2 is higher than from Model M1 (Fig. 10, curves e and b), the abrupt increase of θ_L during the cooling stage must be detected at $T_e < T_i$. The situation is similar if it is considered that $TOF_{ce} > TOF_{ci}$. However, this leads to a lower difference between T_e and T_i which corresponds better to the experimental observations (Fig. 6) as shown in Fig. 10g. The above discussion shows that several experimental data linked to the evolutions of θ_L and TOF during lighting-off tests with 1% CO/x% O_2/He mixtures can be qualitatively well interpreted considering the two kinetic Models M1 and M2. Moreover, TOF_{th} and θ_L from Model M2 (Fig. 10) lead to the conclusion that the Pt–O surface allows performance of the CO/O_2 reaction with TOF values higher by a factor $\gtrsim 100$ as compared to Model M1. In consequence, it is conceivable that Pt-containing catalysts may allow a high CO conversion even at room temperature. However, under classical experimental conditions the Pt–O surface at low reaction temperatures cannot be stabilized to sustain Model M2 and the surface evolves at low temperatures to Pt–CO whatever the CO/O_2 ratio as shown below.

3.8. Study of the Pt–O → Pt–CO transformation at 300 K

The adsorption of O_2 on the freshly reduced catalyst leads to the formation of the Pt–O surface [4]. The introduction of x% CO/He at 300 K removes the O_{sads} as CO_2 and leads to the Pt–O → Pt–CO transformation [4]. We have studied how the Pt–O surface evolves at 300 K using a CO/O_2/He gas mixture in excess O_2. The experiments (Fig. 11) are similar to those performed in [4]: after adsorption of O_2 at 300 K (65 μmol O/g) to form the Pt–O surface followed by a short purge in helium a 0.5% CO/1% O_2/3% Ar/He mixture is introduced. Similarly to previous studies [2,4], C and O mass balances using the curves in Fig. 11A reveal the evolutions of the Pt–O surface with time on stream. At $t \approx 0$, the O_2 signal is high while CO_2 is very low, because L CO species must be formed on the Pt–O surface according to step S1a to produce CO_2. During the following seconds, the O_2 signal decreases showing that O_2 is consumed due to the CO/O_2 reaction (the surface is saturated by O_{sads}) and that during this short period Model M2 is sustained: a fraction of the preadsorbed O_{sads} species removed by steps S3a is replaced by new O_{sads} species according to step S2a. However, step S2a progressively ceases to be operative and the O_2 signal increases to a steady-state value corresponding to the oxidation of CO according to Model M1 (step S2 is operative for the O_2 chemisorption). The O_2 consumption in the negative peak is 57 μmol/g. The CO_2 production: 175 μmol/g is due to (a)

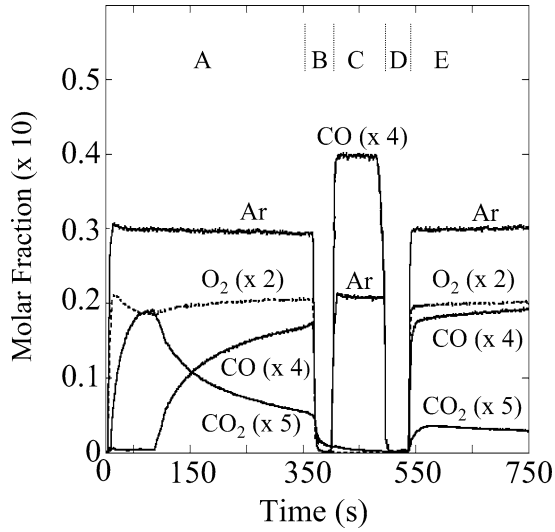

Fig. 11. Molar fractions of the gases in the course of the CO/O_2 reaction at 300 K on Pt–O surface: (A and E) reaction with 0.5% CO/1% O_2/3% Ar/He; (B and D) in helium; (C) titration with 1% CO/2% Ar/He.

the oxidation of CO during the CO/O_2 reaction (the O_2 consumption indicates that $57 \times 2 = 114$ μmol of CO have been oxidized) and (b) the reduction of the preadsorbed O_{sads} species (Pt–O surface) equals to $175–114 = 61$ μmol/g, in agreement with the amount of O_{sads} species adsorbed on a clean Pt surface. The CO consumption during the transient is 244 μmol/g. The comparison with the CO_2 production indicates that $244–175 = 69$ μmol/g of CO have been adsorbed as L CO species in reasonable agreement with the amount of CO adsorbed on a clean stabilized Pt surface.

The C and O mass balances during the first seconds of the CO/O_2 reaction on Pt–O at 300 K indicates that the surface evolves to Pt–CO even in excess O_2 and that there is no more reactive O_{sads} species. This is confirmed by the following experiment: after a helium purge (Fig. 11B) indicating the absence of O_2 and CO desorption, a 1% CO/2% Ar/He mixture is introduced (Fig. 11C). It can be observed that (a) there is no CO_2 production indicating the absence of reactive O_{sads} species on the Pt surface after CO/O_2/He in Fig. 11A and (b) there is no CO adsorption indicating that the Pt surface is saturated by CO during the CO/O_2 reaction in excess O_2. After a helium purge (Fig. 11D), the introduction of the 0.5% CO/1% O_2/3% Ar/He mixture (Fig. 11E) now gives only a small CO_2 production due to the CO/O_2 reaction according to Model M1. The experiments in Fig. 11 show that the Pt–O → Pt–CO transformation at low temperatures is due to three processes: (a) L CO chemisorption is not inhibited on Pt–O; (b) step S3a of Model M2 proceeds with a high rate (in particular S3a is faster than step S3); and (c) L CO on Pt–O inhibits the O_2 chemisorption (i.e., disappearance of the pair sites for dissociative chemisorption) prohibiting that Model M2 is sustained. This Pt–O → Pt–CO transformation occurs whatever P_{O_2} (< 0.5 atm) explaining that only Model M1 is operative during the CO/O_2 reaction before T_i.

3.9. M1 and M2 kinetic models and ignition/extinction processes

Two main explanations are proposed in the literature for the ignition and extinction processes during the CO/O_2 reaction: (a) kinetic models with a competition on the same Pt sites between reactive adsorbed species [32,33] and (b) surface-phase transformations [34,35]. There are other proposals such as the involvement of surface carbon on the Pt surface [36].

3.9.1. Kinetic models with competitive chemisorption

This explanation has been particularly developed by Kaul et al. [33]. The authors have shown that simulations involving (a) a competition between adsorbed CO and oxygen species with kinetic parameters adjusted to obtain a best fit between experimental and theoretical curves and (b) transport processes lead to a good qualitative agreement with several experimental data on ignition/extinction processes such as the decrease in T_i with the increase in P_{O_2}. The ignition/extinction processes appear to be controlled mainly by the competition mechanism while transport processes amplify the differences [33]. We have shown [1–4] studying individually each elementary step of the plausible M1 and M2 kinetic models that there is no competition between the adsorbed species involved in the L-H steps. However, a competition between the B CO species and the oxygen species in Model M1 may exist (not studied).

3.9.2. Surface-phase transformations

This second explanation is related to adsorbate-induced hex ↔ 1 × 1 surface-phase transformations [34] observed on Pt single crystals during CO adsorption and CO/O_2 reaction under UHV conditions [27,35]. These transformations are linked to critical values of the coverage of the adsorbed species. For instance, it is considered that adsorption of CO on clean Pt(100) (hex phase) leads to a transformation to 1 × 1 surface if θ_{CO} on the hex-CO phase exceeds ≈ 0.08 [34,35] and if, in turn, the coverage of the 1×1–CO surface drops below ≈ 0.3 (i.e., during the increase in T_a under isobar conditions) the structure transforms back into the hex phase (the transformation 1 × 1 → hex is an activated process: $E_a \approx 105$ kJ/mol [35]). The driving force for the hex → 1 × 1 transition is the heat of adsorption of CO which is higher by ≈ 42 kJ/mol on the 1 × 1 plane. The two surfaces also present different reactivity for O_2 chemisorption: the sticking coefficient is several orders of magnitude lower on hex than on 1 × 1. Moreover, it is observed that the adsorption of O_2 is strongly inhibited by CO_{ads} on 1 × 1–CO [35] while at the opposite the adsorption of CO on a 1 × 1–O surface is not inhibited as compared to a clean 1 × 1 surface [27,34]. Phase transformations are also observed during the CO/O_2 reaction [35]. The increase in T_r with a $P_{O_2}/P_{CO} \approx 10$ ratio indicates that the surface evolves similarly to the adsorption: there is a phase transformation 1 × 1 → hex at $\theta_{CO} \approx 0.3$. However, in the presence of O_2, this process is associated with a sharp increase in the coverage of the adsorbed oxygen species [35]. These evolutions of the Pt(100) surface during the CO/O_2 reaction are very similar to those observed on the present Pt/Al_2O_3 catalyst with an abrupt change from Pt–CO to Pt–O. However, on Pt/Al_2O_3 there is no phase transformations in the absence of O_2 because the high heats of adsorption of the L CO species [6–10] associated with $P_{CO} > 500$ Pa prevent the critical coverage of ≈ 0.3 at $T_a < 740$ K to be obtained. Under UHV conditions, it is the low P_{CO} values which allow the critical coverage at $T_a < 600$ K to be obtained. During the CO/O_2 reaction in excess O_2 on Pt/Al_2O_3, this critical coverage can be obtained due to the L-H step in association with (a) high TOF values (high CO conversions) and (b) mass-transfer processes in the view of [33].

3.9.3. The ignition process considering Models M1 and M2

To interpret qualitatively this process considering the kinetic models, we adopt the view of single crystals studies [27,35] on a surface phase transformation Pt–CO → Pt–O due to the reactive removal of the L CO species in ex-

cess O_2. The ignition process must be linked to Model M1 that is operative before T_i. For T_r values close to T_i, the calculations using Model M1 indicate that θ_L during the CO/O_2 reaction starts to be slightly affected (as compared to the adsorption equilibrium) by step S3. For instance, at 460 K the adsorption model (expression (2)) leads to $\theta_L = 1$ while Model M1 indicates $\theta_L = 0.998$ for $x = 10$. This may be the trigger for the fast change from Pt–CO to Pt–O. To explain the abrupt decrease in θ_L it must be considered that the ignition process is associated with a high $CO_{\%}$ value (Fig. 2) when mass-transfer processes are operative. These processes limit the concentration of CO at the catalyst surface and step S3 may decrease significantly θ_L, allowing the increase in O_{sads} which in turn contributes to the reactive removal of the L CO species according to S3a of Model M_2. These processes explain that the switch from Model M1 to Model M2 cannot be experimentally followed in excess O_2 studying $\theta = f(T_r)$ because it is associated with high TOF values ($> 1\ s^{-1}$). However, it is more progressive for a stoichiometric CO/O_2 ratio (Fig. 3).

At 300 K the Pt–O → Pt–CO transformation (Fig. 11) is clearly associated with the reduction of the O_{sads} species. Some experimental data support the view that the Pt–CO → Pt–O transformation at the ignition is linked to an oxidative removal of L CO and not to a competitive chemisorption with O_{sads}. The abrupt decrease in θ_L from 1 to ≈ 0.15 at T_i must increase the molar fractions of either CO (i.e., competitive chemisorption [33]) or CO_2 (oxidative removal of L CO) in the gas phase. An estimation of this increase using the experiments with the quartz microreactor (Fig. 7) is performed as follow: (a) the decrease in θ_L from 1 to 0.15 produces ≈ 20 μmol of either CO or CO_2 and (b) FTIR spectra show that this removal is detected at a heating rate of 15 K/min during $t \lesssim 20$ s. This leads to a rate of either CO or CO_2 production of ≈ 1 μmol/s. In parallel, at the ignition the CO conversion is $CO_{\%} \approx 85\%$ and this leads to an apparent CO_2 production rate of 3.5 μmol/s with a 600 cm^3/min flow rate. Roughly, the increase of either CO or CO_2 molar fractions (mass spectrometer) associated with the Pt–CO → Pt–O transformation must be by ≈ 20–30%. Fig. 12 reports $CO_{\%}$ during the light-off test with 1% CO/3% O_2/He using either the CO signal Fig. 12a (identical to Fig. 7b) or the CO_2 signal Fig. 12b. For $CO_{\%} < 60\%$, the two curves are overlapped while for $CO_{\%} > 60\%$, it can be observed that curve b is higher than curve a with a small overshoot at $CO_{\%} = 100\%$. This is the situation expected for the oxidative removal of the L CO species. In excess CO there is no ignition process and curves c and d in Fig. 12 shows that the $CO_{\%}$ curves using either CO or CO_2 are overlapped in the full T_r range for 1% CO/0.25% O_2/He.

The involvement of the reactive removal of either O_{sads} or L CO during the surface transformations can be also justified considering their respective coverage according to a kinetic model assuming (a) a competition on the same Pt^0 sites, (b) the absence of reaction between the two adsorbed species, and (c) that their heats of adsorption are not affected by the coadsorption. Simple calculations (not shown) for 1% CO/1% O_2/He indicate that θ_L is slightly favored at 300 K ($\theta_L \approx 0.56$ and $\theta_{Oads} \approx 0.44$) while the increase in T_a linearly decreases θ_L and in parallel increase θ_{Oads} leading to a situation where θ_{Oads} is favored at high temperatures (i.e., at 700 K: $\theta_L \approx 0.32$ and $\theta_{Oads} \approx 0.68$). These data show that (a) the experimental coverage during the CO/O_2 reaction cannot be explained only by a competitive adsorption and (b) the reactive removal of either L CO or O_{sads} controls the operative Pt surface (Pt–CO or Pt–O).

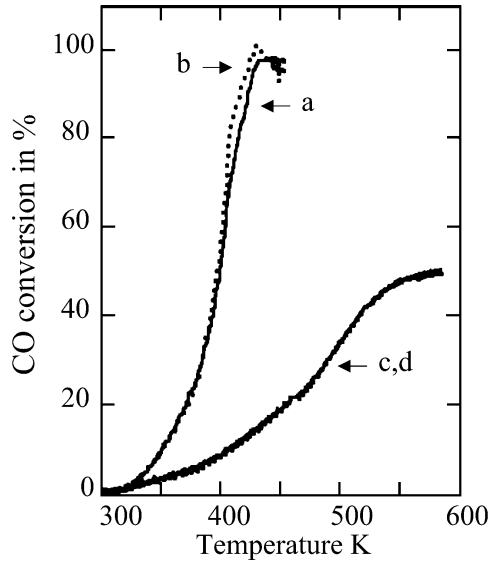

Fig. 12. Comparison of the conversions during light-off tests using 1% CO/x% O_2/He with the quartz microreactor using either the CO and or the CO_2 molar fractions: (a) CO and (b) CO_2 for $x = 3$; (c) CO and (d) CO_2 for $x = 0.25$.

4. Conclusion

In the present study the evolutions on a 2.9% Pt/Al_2O_3 catalyst of (a) the coverage of a linear CO species of Pt^0 sites: θ_L and (b) the TOF during light-off tests (T_r in the range 300–713 K) with 1% CO/x% O_2/He mixtures ($x \leqslant 50$) have been determined by using FTIR and mass spectroscopy. The experimental curves $\theta_L = f(T_r)$ and TOF = $f(T_r)$ have been compared to the theoretical curves obtained from two kinetic Models M1 and M2 deriving from a plausible model with four elementary steps. Models M1 and M2 differ according to the nature of the intermediates species and the kinetic parameters of the elementary steps.

Model M1 implicates [1–3] (a) a L CO species adsorbed on the reduced Pt particles forming a Pt–CO surface (step S1) and (b) a weakly adsorbed oxygen species, O_{wads} (step S2). There is no competition between the L CO and O_{wads} species that react according to a L-H elementary step S3. The desorption of CO_2 (step S4) is fast. The theoretical curves $\theta_L = f(T_r)$ and TOF = $f(T_r)$ obtained from Model M1 using the kinetic parameters previously determined [1–3,6–11] are in good agreement with the experi-

mental curves in the T_r range 300–713 K in excess of CO and in the range 300-T_i in excess of O_2. The specific temperature T_i depends on P_{O_2} and it is characterized by an abrupt decrease in θ_L from ≈ 1 to < 0.15 (ignition process). The agreement between TOF_{ex} and TOF_{th} is limited to CO conversions $\lesssim 15\%$.

In excess O_2, the abrupt decrease in θ_L at T_i is followed by a progressive decrease for $T_r > T_i$. It has been shown that the curves $\theta_L = f(T_r)$, for $T_r > T_i$, agree with Model M2 involving a strongly adsorbed oxygen species O_{sads} (step S3a) on the reduced Pt particles forming a Pt–O surface and a L CO species formed on the Pt–O surface (step S1a). These two species react according to a L-H elementary step S3a. During the cooling stage from $T_r > T_i$ the experimental θ_L values follow the theoretical curve $\theta_L = f(T_r)$ from Model M2 until a value in the range ≈ 0.2–0.3 at a specific temperature $T_e < T_i$ depending on P_{O_2} where an abrupt increase to $\theta_L = 1$ is observed (extinction process) while Model M1 is operative for $T_r < T_e$.

Finally, the ignition/extinction processes are associated with the change in the kinetic model controlling the CO/O_2 reaction: at the ignition M1 $\rightarrow$ M2 and at the extinction M2 $\rightarrow$ M1. These changes are either due or associated with a surface-phase transformation from Pt–CO (M1 model) to Pt–O (M2 model), very similar to the views of single-crystal studies.

The present study and previous works [1–4,6–11] in line with the microkinetic approach of the gas/sold heterogeneous catalysis [5] show that the characterization of the kinetic parameters of each elementary step involved in a plausible mechanism of a catalytic reaction, such as CO/O_2 on Pt/Al_2O_3, constitutes a new way for the understanding of the catalytic activity (TOF) of a catalyst. It is now conceivable that the modifications of the TOF due for instance to the catalyst preparation (i.e., Pt dispersion) can be correlated in future works to a change of a specific kinetic parameter of an elementary step. In line with this view, it has been recently shown that the Pt dispersion has no impact on the heats of adsorption of the L CO species [37].

Acknowledgments

We acknowledge with pleasure FAURECIA Industrie, Bois sur Prés, 25 550 Bavans, France, for its financial support and the MENRT (Ministère de l'Education Nationale, de la Recherche et de la Technologie) for the research fellowship of A. Bourane.

References

[1] A. Bourane, D. Bianchi, J. Catal. 202 (2001) 34.
[2] A. Bourane, D. Bianchi, J. Catal. 209 (2002) 114.
[3] A. Bourane, D. Bianchi, J. Catal. 209 (2002) 126.
[4] A. Bourane, D. Bianchi, J. Catal. 220 (2003) 3.
[5] J.A. Dumesic, et al., The Microkinetics of Heterogeneous Catalysis, 1993, ACS Prof. Ref. Book.
[6] A. Bourane, O. Dulaurent, K. Chandes, Appl. Catal. 214 (2001) 193.
[7] T. Chafik, O. Dulaurent, J.L. Gass, D. Bianchi, J. Catal. 179 (1998) 503.
[8] O. Dulaurent, D. Bianchi, Appl. Catal. 196 (2000) 271.
[9] A. Bourane, O. Dulaurent, D. Bianchi, Langmuir 17 (2001) 5496.
[10] A. Bourane, O. Dulaurent, D. Bianchi, J. Catal. 196 (2000) 115.
[11] A. Bourane, O. Dulaurent, D. Bianchi, J. Catal. 195 (2000) 406.
[12] D.J. Kaul, E.E. Wolf, J. Catal. 89 (1984) 348.
[13] D.J. Kaul, E.E. Wolf, J. Catal. 93 (1985) 321.
[14] J.A. Anderson, J. Chem. Soc., Faraday Trans. 88 (1992) 1197.
[15] D.M. Haaland, F.L. Williams, J. Catal. 76 (1982) 450.
[16] Y. Barshad, X. Zhou, E. Gulari, J. Catal. 94 (1985) 128.
[17] T.H. Lindstrom, T.T. Tsotsis, Surf. Sci. 150 (1985) 487.
[18] F.J. Gracia, J.T. Miller, A.J. Kropf, E.E. Wolf, J. Catal. 209 (2002) 341.
[19] F. Schüth, B.E. Henry, L.D. Schmidt, Adv. Catal. 39 (1993) 51.
[20] Y. Cai, H.G. Strenger Jr., C.E. Lyman, J. Catal. 161 (1996) 123.
[21] S. Glasstone, K.J. Laidler, H. Eyring, The Theory of Rate Processes, McGraw-Hill, New York, 1941.
[22] K.J. Laidler, Catalysis 1 (1954) 75.
[23] D.J. Kaul, E.E. Wolf, Chem. Eng. Sci. 41 (1986) 1101.
[24] S.H. Oh, G.B. Fischer, J.E. Carpenter, D.W. Goodman, J. Catal. 100 (1986) 360.
[25] A. Von Oertzen, A. Mikhailov, H.H. Ritermund, G. Ertl, Surf. Sci. 350 (1996) 259.
[26] J. Hoffmann, I. Meusel, J. Hartmann, J. Libuda, H.J. Freund, J. Catal. 204 (2001) 378.
[27] R. Imbihl, M.P. Cox, G. Ertl, J. Chem. Phys. 83 (1985) 1578.
[28] M. Xu, J. Liu, F. Zaera, J. Chem. Phys. 104 (1996) 8825.
[29] F. Zaera, J. Liu, M. Xu, J. Chem. Phys. 106 (1997) 4204.
[30] M. Lynch, P. Hu, Surf. Sci. 458 (2000) 1.
[31] C.E. Wartnaby, A. Stuck, Y.Y. Yeo, D.A. King, J. Phys. Chem. 100 (1996) 12483.
[32] R.H. Herz, S.P. Marin, J. Catal. 65 (1980) 281.
[33] D.J. Kaul, R. Sant, E.E. Wolf, Chem. Eng. Sci. 42 (1987) 1399.
[34] G. Ertl, Surf. Sci. 152 (1985) 328.
[35] R. Imbihl, M.P. Cox, J. Chem. Phys. 84 (1986) 3519.
[36] V.A. Burrows, S. Sundaresan, Y.J. Chabal, S.B. Christman, Surf. Sci. 180 (1987) 110.
[37] A. Bourane, D. Bianchi, J. Catal. 218 (2003) 447.